INTERNATIONAL JOURNAL FOR NUMERICAL METHODS IN ENGINEERING

Int. J. Numer. Meth. Engng 2000; **00**:1–6 *Prepared using* nmeauth.cls *[Version: 2002/09/18 v2.02]*

Singularity enrichment for complete sliding contact using the partition of unity finite element method

E. Giner[1,*], N. Sukumar[2], F. J. Fuenmayor[1] and A. Vercher[1]

[1] *Departamento de Ingeniería Mecánica y de Materiales, Universidad Politécnica de Valencia, E–46022 Valencia, Spain.*

[2] *Department of Civil and Environmental Engineering, University of California, One Shields Avenue, Davis, CA 95616, USA.*

SUMMARY

In this paper, the numerical modelling of complete sliding contact and its associated singularity is carried out using the partition of unity finite element method. Sliding interfaces in engineering components lead to crack nucleation and growth in the vicinity of the contact zone. To accurately capture the singular stress field at the contact corner, we use the partition of unity framework to enrich the standard displacement-based finite element approximation by additional (enriched) functions. These enriched functions are derived from the analytical expression of the asymptotic displacement field in the vicinity of the contact corner. In order to characterize the intensity of the singularity, a domain integral formulation is adopted to compute the generalized stress intensity factor. Numerical results on benchmark problems are presented to demonstrate the improved accuracy and benefits of this technique. We conduct an investigation on issues pertaining to the extent of enrichment, accurate numerical integration of weak form integrals, and the rate of convergence in energy. The use of partition of unity enrichment leads to

*Correspondence to: Eugenio Giner, Departamento de Ingeniería Mecánica y de Materiales, Universidad Politécnica de Valencia, E–46022 Valencia, Spain. E-mail: eginerm@mcm.upv.es

Contract/grant sponsor: Ministerio de Educación y Ciencia and Generalitat Valenciana, Spain; contract/grant number: DPI2007-66995-C03-02 and GV06/124.

accurate estimations of the generalized stress intensity factors on relatively coarse meshes, which is particularly beneficial for modelling non-linear sliding contact.

KEY WORDS: sliding contact; singularity enrichment; partition of unity; extended finite element method; domain integral

1. INTRODUCTION

In engineering components, friction along sliding interfaces is a common occurrence, which may lead to crack nucleation and growth, a phenomenon known as fretting fatigue [1]. More specifically, fretting fatigue problems arise when two mechanical components are in contact under the action of normal forces and simultaneously undergo relative displacements of small amplitude. Under these conditions, the stresses are steep in the vicinity of the contact zone. These gradients combined with their cyclic evolution lead to the nucleation of small cracks that often grow under fatigue loads until failure of the component (hence the term fretting fatigue). Examples can be found in riveted or bolted joints, shrink-fit assemblies, hub-axle joints, spline shafts such as those used in gas turbines, etc.

When the size of the contact zone does not depend on the normal load applied to the components, the contact is said to be complete and the stress state at the corners of the contact zone is usually singular for linear elastic media. In fact, two different situations can arise: the region next to the contact corner can be either adhered or slipping. Furthermore, this contact condition can vary over a loading cycle. The distribution of the elastic fields near the end of the contact for the adhered case was given by Williams [2]. For the sliding condition (the case considered in this study), the corresponding stress and displacement fields, which are due to Gdoutos and Theocaris, and Comninou, can be found in References [3, 4, 5].

Two parameters are used to describe the singular fields: the eigenvalue, λ, which represents the order of the singularity, and a multiplier constant, the so-called generalized stress intensity factor (GSIF), K^C, which is analogous to the stress intensity factor in linear elastic fracture mechanics (LEFM). The eigenvalue, λ, is usually known in advance whereas the GSIF is numerically computed, for instance, using the finite element (FE) method. For points sufficiently close to the singularity, the stress field can be expressed as

$$\sigma_{ij} \propto K^C r^{\lambda-1}, \tag{1}$$

where r is the radial distance to the contact corner. We use a specially conceived domain integral to compute K^C from the numerical solution of the elastic problem [6]. The path-independent contour integral is recast in domain form for the sliding contact problem [7, 8], and is better-suited for post-processing in a FE analysis. In previous studies [6, 7, 8], this integral has provided accurate estimations of the GSIF.

In this study, we use the partition of unity framework (PU) to introduce additional functions (enrichment functions) in the FE formulation. The use of known functions to better capture the local character of a solution in the vicinity of a discontinuity, singular point or line, etc., has come to prominence in FE analysis during the last decade. Melenk and Babuška [9, 10] set the mathematical foundations of the procedure. One of the most widespread applications of this approach has been in modelling strong discontinuities, as in Reference [11] and especially in the extended finite element method [12, 13] and the generalized finite element method [14], that have proved to be successful in 2- and 3-dimensional LEFM. In Reference [15], partition of unity enrichment for a crack impinging on a bimateral interface is proposed, whereas in Reference [16], PU enrichment for bimaterial interfacial cracks is introduced. In a similar vein, in this study we adopt the partition of unity framework to better capture the stress singularity that exists in complete sliding contact problems.

In this work, we show that the proposed enrichment technique yields accurate estimates of the GSIF on relatively coarse meshes, since the analytical description of the singular field is embedded in the FE approximation. The advantages of this approach are two-fold: first, use of coarse meshes to accurately estimate the GSIF is pertinent for modelling non-linear sliding contact problems since such problems are computationally demanding. Secondly, the proposed formulation enables the modelling of the singular point at any arbitrary location along the contacting surface. This introduces an important advantage over previous finite element techniques, which are based on the use of special singular elements [17, 18] that are restricted to fixed locations (chosen *a priori*) in the FE analysis.

The remainder of this paper is organized as follows. In the next section, a brief description of the elastic fields that characterize complete sliding contact is given. Then, we briefly touch upon the domain integral formulation that is used to compute the GSIF. In Section 4, the PU enrichment for complete sliding contact is introduced, and a few particulars of its numerical implementation within ABAQUS^{TM} are indicated. A benchmark problem and the corresponding numerical verification are presented in Section 5, with assessment of the rate of convergence in strain energy and the error in the GSIF due to enrichment. In addition, the effect of numerical quadrature is also studied. A second numerical example is presented to demonstrate the accuracy and performance of the method in a sliding contact problem. Finally, some concluding remarks are mentioned in Section 6.

2. FRICTIONAL COMPLETE CONTACT IN GLOBAL SLIDING

The elastic fields present around the edge of the frictional contact between a sliding wedge and a half-plane were analyzed by Gdoutos and Theocaris [3] and Comninou [4] using asymptotic analysis. They studied the frictional contact problem for indenters elastically dissimilar to the contacting surface. More recently, Mugadu *et al.* [5] specialized these results to fretting fatigue applications, where the

same material for both contacting bodies is assumed.

Now, the classical solution of the frictional contact problem with global sliding condition between a wedge and a half-plane is summarized. It is assumed that the bodies are elastically similar, isotropic, and homogeneous. Figure 1 shows the end of the contact zone. A polar co-ordinate system is defined, with origin at the end of the contact plane. The wedge angle is denoted by ψ and f is the coefficient of friction.

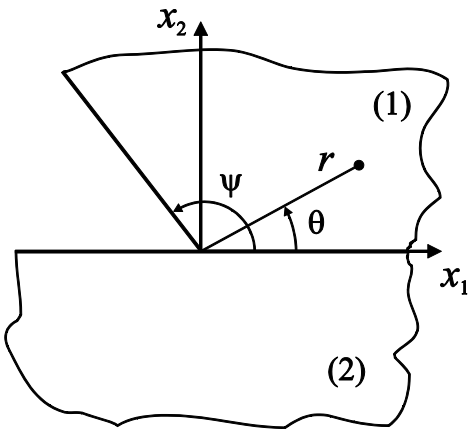

Figure 1. The problem of a sliding wedge on a contact plane with friction.

The stress fields $\sigma^{(i)}$ and displacement fields $u^{(i)}$ for each of the bodies $^{(i)}$, $i = 1, 2$, can be obtained from the Airy functions $\varphi^{(i)}$ that satisfy the boundary conditions for both contacting bodies, as detailed for example in References [5, 6]. In each body, the Airy function satisfies the biharmonic equation

$$\nabla^4 \varphi^{(i)} = 0. \tag{2}$$

The solution of this equation has the following form:

$$\varphi^{(i)}(r,\theta) = r^{\lambda+1}\left(a^{(i)}\mathrm{s}_+\theta + b^{(i)}\mathrm{c}_+\theta + c^{(i)}\mathrm{s}_-\theta + d^{(i)}\mathrm{c}_-\theta\right), \tag{3}$$

where the following definitions are used: $\mathrm{s}_+\theta = \sin(1+\lambda)\theta$, $\mathrm{s}_-\theta = \sin(1-\lambda)\theta$, $\mathrm{c}_+\theta = \cos(1+\lambda)\theta$ and $\mathrm{c}_-\theta = \cos(1-\lambda)\theta$. In addition, $a^{(i)}$, $b^{(i)}$, $c^{(i)}$ and $d^{(i)}$ are eight unknowns to be determined using the boundary conditions for each body. From Figure 1, the natural boundary conditions are zero-traction on the free-boundary of the bodies:

$$\begin{aligned} \sigma^{(2)}_{\theta\theta}(r,-\pi) &= 0, \\ \sigma^{(2)}_{r\theta}(r,-\pi) &= 0, \\ \sigma^{(1)}_{\theta\theta}(r,\psi) &= 0, \\ \sigma^{(1)}_{r\theta}(r,\psi) &= 0, \end{aligned} \tag{4}$$

and the traction and displacement continuity conditions at the common boundary are

$$\begin{aligned} \sigma^{(2)}_{r\theta}(r,0) + f\sigma^{(2)}_{\theta\theta}(r,0) &= 0, \\ \sigma^{(1)}_{r\theta}(r,0) + f\sigma^{(1)}_{\theta\theta}(r,0) &= 0, \\ \sigma^{(2)}_{\theta\theta}(r,0) - \sigma^{(1)}_{\theta\theta}(r,0) &= 0, \\ u^{(2)}_{\theta}(r,0) - u^{(1)}_{\theta}(r,0) &= 0. \end{aligned} \tag{5}$$

The parameter f is the coefficient of friction. It can take a positive value (if the slip of the wedge is in the positive x_1-direction) or a negative value (if the slip is in the negative x_1-direction).

A system with eight equations and eight unknowns is obtained when using the relationships between the Airy stress functions and the polar components of stress and displacement [6, 19], combined with Equations (4) and (5). In the derivation, it is convenient to use the Michell solution for the polar components of displacements (see [19]).† The system is of the form:

$$\begin{bmatrix} [A_{11}] & [A_{12}] \\ [A_{21}] & [A_{22}] \end{bmatrix} \begin{Bmatrix} \{k^{(1)}\} \\ \{k^{(2)}\} \end{Bmatrix} = \begin{Bmatrix} \{0\} \\ \{0\} \end{Bmatrix}, \tag{6}$$

where $\{k^{(i)}\} = \{a^{(i)}\ b^{(i)}\ c^{(i)}\ d^{(i)}\}^{\mathrm{T}}$ are the eight unknowns to be solved. The submatrices $[A_{ij}]$ in

†The same result can be obtained using the Mellin transform instead, as in Reference [5].

Equation (6) can be found in References [6, 8]. In order to solve for the displacement and stress fields, a non-trivial solution of the homogeneous system given in Equation (6) must be found. The system has a non-trivial solution if and only if its determinant is equal to zero. Therefore, the following characteristic equation is obtained:

$$\begin{aligned}\Delta(\lambda) = &\cos(\lambda\pi)\left(\sin^2\lambda\psi - \lambda^2\sin^2\psi\right) + \\ &0.5\sin(\lambda\pi)\left(\sin 2\lambda\psi + \lambda\sin 2\psi\right) + \\ &f\lambda(1+\lambda)\sin(\lambda\pi)\sin^2\psi = 0.\end{aligned} \tag{7}$$

The roots of the characteristic equation are the eigenvalues λ_j ($j = 1, \ldots, \infty$). Given an eigenvalue λ_j, the system of equations (6) is used to solve the eigenvector problem for $\lambda = \lambda_j$ and to find the constants $a_j^{(i)}$, $b_j^{(i)}$, $c_j^{(i)}$ and $d_j^{(i)}$. The displacement field is then computed as

$$\left\{u^{(i)}(r,\theta)\right\} = \left\{\begin{array}{c} u_r^{(i)} \\ \\ u_\theta^{(i)} \end{array}\right\} = \sum_{j=1}^{\infty} K_j^C r^{\lambda_j}\left\{\Psi_j^{(i)}(\theta,\lambda_j)\right\} \tag{8}$$

with

$$\left\{\Psi_j^{(i)}(\theta,\lambda_j)\right\} = \frac{1}{2\mu}\left\{\begin{array}{l} -(\lambda_j+1)(a_j^{(i)}\mathrm{s}_+\theta + b_j^{(i)}\mathrm{c}_+\theta) + (\kappa-\lambda_j)(c_j^{(i)}\mathrm{s}_-\theta + d_j^{(i)}\mathrm{c}_-\theta) \\ (\lambda_j+1)(-a_j^{(i)}\mathrm{c}_+\theta + b_j^{(i)}\mathrm{s}_+\theta) + (\kappa+\lambda_j)(c_j^{(i)}\mathrm{c}_-\theta - d_j^{(i)}\mathrm{s}_-\theta) \end{array}\right\}, \tag{9}$$

where κ is the Kolosov's constant ($\kappa = 3 - 4\nu$ for plane strain and $\kappa = (3-\nu)/(1+\nu)$ for plane stress), ν is the Poisson's ratio and μ is the shear modulus of the material. In addition, the singular stress field is expressed as:

$$\left\{\sigma^{(i)}(r,\theta)\right\} = \left\{\begin{array}{c} \sigma_{rr}^{(i)} \\ \\ \sigma_{\theta\theta}^{(i)} \\ \\ \sigma_{r\theta}^{(i)} \end{array}\right\} = \sum_{j=1}^{\infty} K_j^C r^{\lambda_j - 1}\left\{\Phi_j^{(i)}(\theta,\lambda_j)\right\}, \tag{10}$$

where

$$\left\{\Phi_j^{(i)}(\theta,\lambda_j)\right\} = \left\{ \begin{array}{c} \lambda_j(\lambda_j+1)\left(-a_j^{(i)}\mathrm{s}_+\theta - b_j^{(i)}\mathrm{c}_+\theta\right) + \lambda_j(\lambda_j-3)\left(-c_j^{(i)}\mathrm{s}_-\theta - d_j^{(i)}\mathrm{c}_-\theta\right) \\ \lambda_j(\lambda_j+1)\left(a_j^{(i)}\mathrm{s}_+\theta + b_j^{(i)}\mathrm{c}_+\theta + c_j^{(i)}\mathrm{s}_-\theta + d_j^{(i)}\mathrm{c}_-\theta\right) \\ \lambda_j(\lambda_j+1)\left(-a_j^{(i)}\mathrm{c}_+\theta + b_j^{(i)}\mathrm{s}_+\theta\right) + \lambda_j(1-\lambda_j)\left(-c_j^{(i)}\mathrm{c}_-\theta + d_j^{(i)}\mathrm{s}_-\theta\right) \end{array} \right\}. \tag{11}$$

The traction vector $T_k^{(i)}$ is defined as $\sigma_{jk}^{(i)} n_j$, where the stress components are defined in Equation (10) and n_k is the normal vector to a given contour.

3. DOMAIN INTEGRAL FOR GSIF EXTRACTION

As indicated in Section 2, the GSIFs are the multiplier constants K_j^C that scale the intensity of the elastic fields in Equations (8) and (10). For a given problem, λ_j can be computed in advance by solving the characteristic equation (7). However, the GSIFs are generally unknown because they depend on the specific boundary conditions of the problem. This usually implies that numerical methods must be used to approximate the elastic fields, followed by post-processing techniques to extract the GSIFs. In practice, the first term in the expansion series in Equations (8) and (10) (singular term) dominates the elastic fields, so the value K_1^C (denoted here simply as K^C) is the quantity of interest. Collocation procedures, like the stress or displacement extrapolation techniques have been used in the literature [17], but they need very refined meshes and sufficient user-intervention that renders it difficult to conduct a systematic study. An efficient way of extracting K^C from a FE solution is the special domain integral presented in Reference [6]. We now present the essentials of this formulation.

Figure 2 shows the singular point surrounded by a domain Ω^*. The domain integral method yields the value of K^C by performing the following integration over the domain Ω^*:

$$K_j^C = -\frac{1}{C_{j,E}} \int_{\Omega^*} \left(\sigma_{kl}^h u_l^E - \sigma_{kl}^E u_l^h\right) \frac{\partial q}{\partial x_k}\, \mathrm{d}\Omega. \tag{12}$$

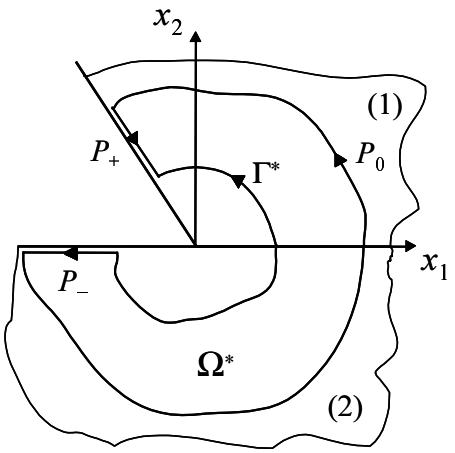

Figure 2. Domain region Ω^* over which the integration is performed.

The contour integral that leads to the domain integral (12) was proposed in References [7, 8]. It is path-independent, yielding the same result when the paths Γ^* and P_0 defined in Figure 2 are traversed. In practice, this independence is not exact due to the discretization error. This contour integral is based on Betti's Reciprocal Theorem. In Reference [6], this integral is recast into the domain integral form shown in Equation (12), where u_l^h, σ_{kl}^h are the elastic fields obtained via a finite element analysis and u_l^E, σ_{kl}^E are the extraction fields specially conceived for this type of problem, and are defined in References [6, 7, 8]. The constant $C_{j,E}$ that relates the jth term of the series expansion and the extraction field E is defined as

$$C_{j,E} = \int_{-\pi}^{\psi} \left(\lambda_j \{\Xi_j\}^{\mathrm{T}} \{\Psi_E\} + \lambda_E \{\Xi_E\}^{\mathrm{T}} \{\Psi_j\}\right) \mathrm{d}\theta, \tag{13}$$

where Ψ_j, Ξ_j are the trigonometric functions that are associated with the displacement field given in Equation (9) and the traction vector $T_k = \sigma_{jk} n_j$ (derived from Equation (10)), respectively.

The gradient of the so-called q-function is a factor in the integrand as a result of the conversion into a domain integral, which is analogous the domain integral form of the J-integral in LEFM. The function

$q(x_1, x_2)$ can be any continuous function, provided that it is zero on the outer contour Γ_0 and the external region. In addition, q must be 1 on the inner contour Γ^* and the region enclosed. The q-function is a mere mathematical function that allows the recast into a domain integral and only the region where the gradient of q is non-zero (i.e. Ω^*) will contribute to the domain integral in Equation (12). Within the limits of finite element discretization errors, the domain integral yields a value that is independent of Ω^*. In Reference [6], it is concluded that the elements closest to the singular point should not be included in Ω^* due to the large discretization error that is present in these elements. The simplicity and high-accuracy of the domain integral formulation renders it to be well-suited for use within the PUFE method.

4. PARTITION OF UNITY FINITE ELEMENT APPROXIMATION

To better capture the local character of the sliding contact solution in the vicinity of the singular point, we enrich the finite element approximation. This is accomplished using the partition of unity framework, and follows previous applications in LEFM [12]. In a standard FE formulation, the displacement approximations (trial functions) are written as:

$$\mathbf{u}^h(\mathbf{x}) = \sum_{i \in I} \phi_i(\mathbf{x}) \mathbf{u}_i \tag{14}$$

where I is the set of all nodes in the domain, and $\mathbf{u}_i$ is the solution at node i and ϕ_i is the corresponding basis function. The trial space for each displacement component is then $\mathtt{span}\{\phi_i\}_{i \in I}$, and it is well-known that the finite element basis functions form a partition of unity: $\sum \phi_i(\mathbf{x}) = 1$. The essential feature of the PU method is the multiplication of the nodal basis functions $\phi_i(\mathbf{x})$ with *enrichment functions* $F(\mathbf{x})$. If we define J as the subset of enriched nodes, $J \subset I$, then the enriched approximation

using the PU framework is [9]:

$$\mathbf{u}^h(\mathbf{x}) = \sum_{i\in I} \phi_i(\mathbf{x})\mathbf{u}_i + \sum_{j\in J} \phi_j(\mathbf{x}) \left(\sum_{\alpha} F_\alpha(\mathbf{x})\mathbf{a}_{j\alpha} \right), \tag{15}$$

where $F_\alpha(\mathbf{x})$ are a set of enrichment functions that are included at each enriched node $j \in J$, together with new degrees of freedom $\mathbf{a}_{j\alpha}$. The trial space is now augmented by $\mathtt{span}\{\phi_j F_\alpha\}_{j\in J}$. Following this approach, the enriched bases inherit properties of the FE basis functions, such as their compact support, and hence preserves many of the advantages of the FEM, like the symmetry and sparsity of the stiffness matrix. In addition, this allows a straightforward implementation of this technique within a FE-based code. Owing to the partition of unity property, the ability to represent rigid body translation and constant strain modes is retained (sufficient conditions for convergence). In contrast, other approaches that include power type singularities within special finite elements [20] cannot meet these conditions.

The first term of the analytical displacement fields given in Equations (8) and (9) is the term of interest, since it constitutes the dominant singular term in the expression for the stress field. This first term is of the form:

$$\left\{ \begin{array}{c} u_r^{(i)} \\ u_\theta^{(i)} \end{array} \right\} = K^C r^\lambda \frac{1}{2\mu} \left\{ \begin{array}{l} -(\lambda+1)(a^{(i)}\mathrm{s}_+\theta + b^{(i)}\mathrm{c}_+\theta) + (\kappa-\lambda)(c^{(i)}\mathrm{s}_-\theta + d^{(i)}\mathrm{c}_-\theta) \\ (\lambda+1)(-a^{(i)}\mathrm{c}_+\theta + b^{(i)}\mathrm{s}_+\theta) + (\kappa+\lambda)(c^{(i)}\mathrm{c}_-\theta - d^{(i)}\mathrm{s}_-\theta) \end{array} \right\} \tag{16}$$

where the subscript $j = 1$ has been dropped for the sake of simplicity. Expressing these polar components of the displacement field in the vicinity of the singular point as Cartesian components and after algebraic manipulation, the following enrichment functions (these span the dominant term in the analytical displacement field) are obtained:

$$[F_\alpha(r,\theta),\ \alpha = 1\text{–}4] = r^\lambda \left[\sin\lambda\theta,\ \cos\lambda\theta,\ \sin(\lambda-2)\theta,\ \cos(\lambda-2)\theta\right] \tag{17}$$

These functions are the same for both solids, and are used in the enriched approximation given in

Equation (15). We note in passing that the span of these enrichment functions has the same form as those used for a crack impinging a bimaterial interface [15, 21].

Figure 3 shows the enriched nodes for a given configuration of both contacting solids. The enriched nodes are the nodes located at the singular point together with the surrounding nodes. In other words, the enriched nodes are those whose basis function support includes the singular point. Depending on the position of the indenter (solid 1) on the substrate (solid 2), the number of enriched nodes may vary. The elements that contain at least one enriched node will be called enriched elements. According to Equation (15), every enriched node $j \in J$ has 10 degrees of freedom (dof): two standard dof (the two components of the vector $\mathbf{u}_j$) and eight extra dof $\mathbf{a}_{j\alpha}$, where $\mathbf{a}_{j\alpha}$ is the two-component vector for each enrichment function F_α, with $\alpha = 1$–4. To illustrate the effect of the enrichment functions on the trial space, Figure 4 shows plots of $\phi_1 F_2$ and $\phi_1 F_4$ corresponding to the node located at the singular vertex of the indenter (denoted as node 1 in Figure 4). Note the steep gradient in the vicinity of the vertex node that gives rise to the strong singular behaviour in stresses and the compact support feature inherited from the basis function ϕ_1.

4.1. Implementation

The implementation of the enrichment has been carried out in the commercial code ABAQUS™. Taking advantage of the user element capability of this code, we have defined a new user element that includes the proposed enrichment in its formulation, allowing 10 dofs per enriched node. In this way, we benefit from the contact algorithms implemented in the code, as well as from the built-in pre- and post-processing features.

Figure 5 shows a comparison of contour plots using standard FE and the enriched implementation in ABAQUS. The results are obtained using the benchmark problem described in Section 5 and are

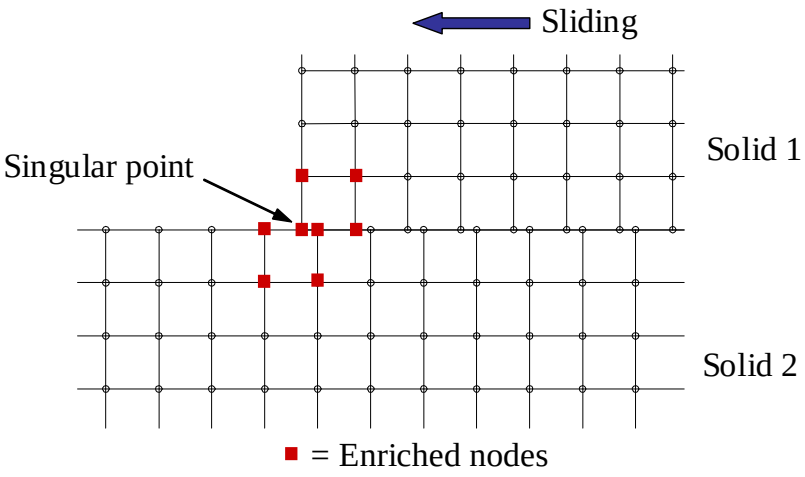

Figure 3. Enriched nodes belonging to elements that contain the singular point.

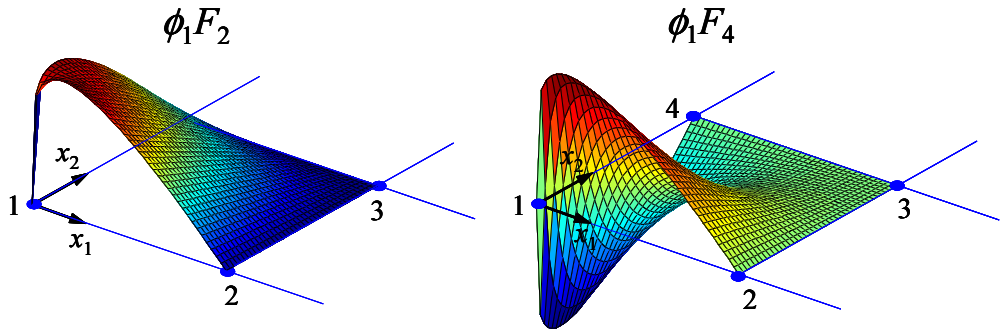

Figure 4. Plots of $\phi_1 F_2$ and $\phi_1 F_4$ corresponding to the node located at the singular vertex of the indenter.

specialized here for a given strain component ε_{11}. In this example, the singular point coincides with a node of the substrate. Therefore, the number of enriched elements is 4 for the indenter and 8 for the substrate. An important limitation of user elements in ABAQUS is that they cannot be represented in any post-processing plots. This is shown in the center plot in Figure 5, where the four and eight enriched elements of the indenter and substrate, respectively, cannot be plotted. ABAQUS simply marks with

a cross the position of the first node in the connectivity of the enriched element. Of course, this first node in the connectivity is not necessarily an enriched node. As is apparent from Equation (15), the displacement approximation at an enriched node j, $\mathbf{u}^h(\mathbf{x}_j)$ is given by the contribution of the standard dof $\mathbf{u}_j$ and the extra dof $F_\alpha \mathbf{a}_{j\alpha}$. Since ABAQUS only uses the standard dof $\mathbf{u}_j$ to represent the displacement in the physical co-ordinates, the deformed position of the first nodes in the connectivity of the enriched elements has no physical meaning, as can be seen in the center plot of Figure 5.

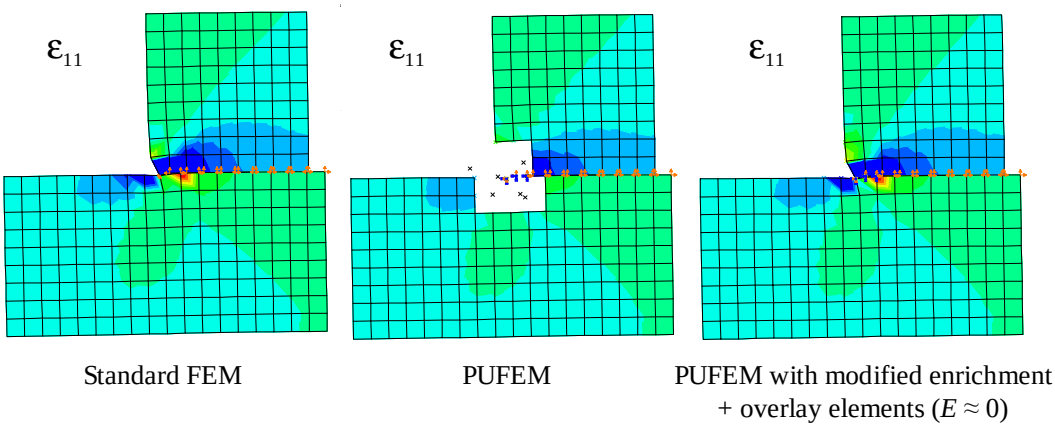

Figure 5. Implementation using ABAQUS. Comparison of contour plots for a given field ε_{11}: left, standard FEM without any enrichment. Center, enrichment with user elements in ABAQUS. Right, modified enrichment with user elements and overlay elements.

To overcome this problem, the following approach has been used. The enriched approximation given in Equation (15) is modified as in Reference [22]:

$$\mathbf{u}^h(\mathbf{x}) = \sum_{i\in I} \phi_i(\mathbf{x})\mathbf{u}_i + \sum_{j\in J} \phi_j(\mathbf{x}) \left(\sum_{k=1}^{4} \left[F_\alpha(\mathbf{x}) - F_\alpha(\mathbf{x}_j) \right] \mathbf{a}_{j\alpha} \right) \tag{18}$$

where $\mathbf{x}_j$ are the nodal co-ordinates of the enriched node j. Therefore, the contribution of the enrichment functions cancels at the enriched node (but not at any other point, such as the integration points). Note also that $F_\alpha(\mathbf{x}_j)$ are singled-valued in the present application and Equation (18)

introduces no ambiguity. As a consequence, the values of the standard dof $\mathbf{u}_j$ will contain the physical displacements. This enables a representation of the deformed configuration of the enriched elements in ABAQUS. We use standard 4-node linear elements with negligible stiffness connected to the nodes of every enriched element, retaining the same connectivity, and hence, overlapping them. We refer to these dummy elements as *overlay elements*. Therefore, a plot of the displacement or strain field using overlay elements will result in bilinear interpolation of the nodal values within these elements (see the rightmost plot in Figure 5). We point out that due to the negligible stiffness of the overlay elements, the stress field is virtually zero within them and hence a contour plot of the enriched stress field would not be very revealing.

It is clear that this added capability in the post-processing of the enriched solution is of interest. The use of overlay elements also plays a critical role in this study: all the node-to-surface contact interactions in the model are established using only the standard and overlay elements (ABAQUS cannot handle contact interactions between user-elements). As the modified enrichment approach of Equation (18) is implemented, and since ABAQUS uses the standard dof $\mathbf{u}_j$ during the non-linear analysis stage, the updated positions of the nodal co-ordinates correspond to the desired physical co-ordinates. This procedure has proved to be robust and has allowed us to combine user-elements with the contact capabilities within ABAQUS. In this way a sliding contact problem with friction can be modelled in combination with the enriched formulation, as exemplified in Section 5.2. Note that the sliding of the singular corner on the substrate implies a redefinition of the enriched nodes of the substrate as the corner changes its position. The enriched nodes of the indenter remain unchanged.

5. NUMERICAL EXAMPLES

In this section, we show that the proposed enrichment yields better estimates of the GSIF on relatively coarse meshes compared to standard finite elements. In assessing the accuracy of the technique, a difficulty that arises is the lack of a suitable benchmark sliding contact problem that can serve as a reference. For this reason, we have considered the following benchmark problem: a finite portion of the domain of the two bodies with the imposition of the exact singular field on the boundaries (Problem 1). This is equivalent to solving two separate linear elastic singular problems, because the contact interaction is not considered and is substituted by the exact displacements of the singular field. We have also applied the enrichment to a true sliding contact problem (Problem 2), taking the solution provided by the standard FEM with a very refined mesh as the reference solution.

5.1. Problem 1: Benchmark problem

5.1.1. Problem description. Figure 6 shows a deformed configuration of the benchmark FE model used in this work. We have taken a finite portion of the two bodies and imposed the exact singular field on their boundaries, just as if they were two separate elastic solids. We have applied exact displacements (Dirichlet boundary conditions) on the contacting sides. For the enriched elements on the contacting side, the exact displacements are applied in accordance to the displacement interpolation (15). For the non-enriched elements on the contacting side, the exact solution is imposed in a weak form. On the rest of the boundary, exact tractions are imposed respecting the two traction-free sides.

The indenter angle ψ is 90° (see Figure 1) and the value of the friction coefficient is $f = -1.6$. The minus sign indicates that the sliding direction of the indenter is to the left (i.e., the corner of interest is a leading corner). Note that the same corner can have a different behaviour when it slides to the right (trailing corner), implying a positive f. On solving the characteristic equation (7), the eigenvalue λ is

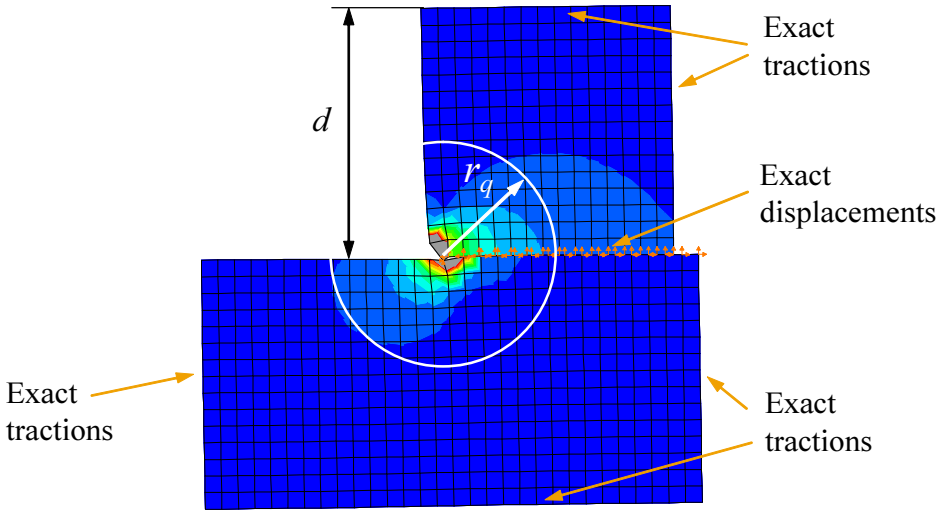

Figure 6. Benchmark problem used for evaluating the performance of the proposed enrichment. r_q is the radius of the q-function for evaluating the domain integral. Shown: mesh 2 of the sequence.

obtained as the smallest positive root: $\lambda = 0.17944$. The relatively high value of the friction coefficient and the corresponding small value of λ lead to a strong singular stress field:

$$\sigma \propto r^{0.179-1}, \tag{19}$$

which is much stronger than, for example, the singularity in LEFM ($\sigma \propto r^{0.5-1}$). The material is assumed to have a linear elastic behaviour, with $E = 210000$ (units of pressure) and $\nu = 0.3$. The singular field imposed corresponds to the first term of the expansions given in Equations (8) and (10). We have assumed a GSIF, $K^C_{\text{exact}} = 1$, as the exact reference solution for the subsequent analyses.

In this study, the q-function is defined as in Reference [12]: all nodes within a circle of radius r_q centered at the singular point take the value of 1 (see Figure 6). At the rest of nodes, $q = 0$. Therefore, only elements traversed by the circumference r_q have a non-zero gradient of q and contribute to the domain integral in Equation (12). The q-function in these elements is defined via bilinear finite element interpolation within the element. Note that the dimensions of the indenter (height d) limits the range of

r_q. The results that follow are presented for several values of r_q scaled with respect to d.

5.1.2. GSIF values for a sequence of uniform meshes. To verify the improvement in the GSIF extraction when using enrichment functions, a sequence of six uniformly refined meshes has been analyzed. The ratios of the element size h to the height d of the indenter are $1/9$, $1/15$, $1/30$, $1/45$, $1/60$ and $1/90$. The mesh shown in Figure 6 corresponds to mesh number 2, with 1504 dof. For each mesh, the domain integral has been applied with different ratios of r_q/d both to a standard and enriched FE solutions, enabling the assessment of the proposed enrichment.

Figure 7 shows the GSIF estimations obtained with the domain integral for the sequence of six meshes. The number of dof for each mesh refers to the standard FE solution. For the enriched solution with topological enrichment (which is usually the first choice), the number of dof is increased by 80, since only 10 nodes are enriched: two nodes at the singular point (indenter and substrate) plus three and five surrounding nodes, respectively. Following the strategy presented in References [23] and [24], the sequence of uniform meshes has also been enriched geometrically (i.e., the enriched nodes are those located within a fixed area surrounding the singular point). The chosen fixed region is a circle of radius $0.213d$.

As the reference solution is $K^C_{\text{exact}} = 1$, it can be seen that the enriched FE solutions provide a better estimation of the GSIF than the standard FEM, both for all meshes and for all ratios r_q/d. As expected, the standard and the enriched solutions tend to converge as the refinement of the mesh increases. Note also that although the domain integral should be theoretically independent of the radius r_q, there is a slight dependency on r_q which is stronger for coarse meshes due to the discretization error. In the first three meshes, low values of r_q/d imply that only the closest elements to the singular point are computed in the domain integral. This yields less accurate estimations of the GSIF for both the standard FE and the topologically enriched solution. The vertical lines in the plots for meshes 1 and 2 mark the extent of

the enriched elements in the topological enrichment case. Nevertheless, the GSIF estimation is always better for the enriched solution, including the cases in which the domain integral is computed only within the enriched elements.

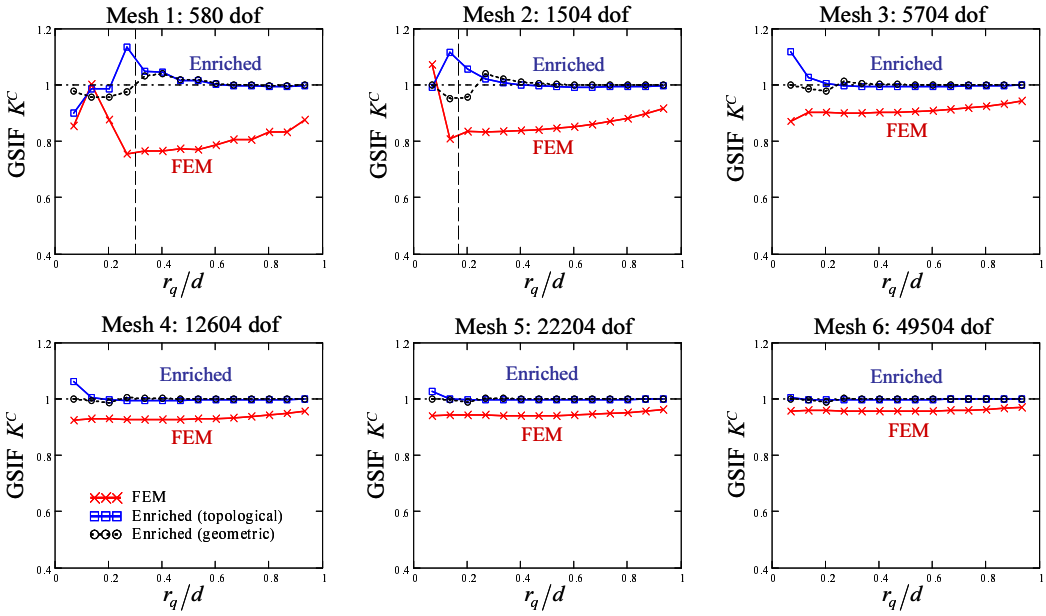

Figure 7. Estimations of the GSIF for a sequence of uniformly refined meshes, comparing the enriched and the standard FE solution. The exact reference value is 1. Estimations are given for different radii of the q-function.

5.1.3. Error in energy norm and in GSIF. The same sequence of six uniformly refined meshes is used to study the error in energy norm and in the quantity of interest K^C, and hence evaluate their convergence rates. It is well known that the error in energy norm of a standard FE solution of a singular problem with a uniform mesh refinement is bounded by

$$\|\mathbf{e}\|_E \leq Ch^{\min(p,\lambda)}, \tag{20}$$

where $\mathbf{e} = \mathbf{u} - \mathbf{u}^h$ is the error in displacements introduced by the finite element approximation, C is a constant that depends on the problem, h is the characteristic element size, p is the order of the elements used in the discretization and λ is the eigenvalue related to the order of the singularity introduced in previous sections. In this work, we will use the square of the error in the energy norm (which is related to the error in strain energy) and therefore

$$\|\mathbf{e}\|_E^2 \leq C^2 h^{2\min(p,\lambda)} = C^2 h^{2\lambda}. \tag{21}$$

Since $\lambda = 0.17944$ in our problem, the theoretical rate of convergence of $\|\mathbf{e}\|_E^2$ is $2\lambda = 0.35888$. The results are plotted in Figure 8 (left) for the six meshes. It can be seen that the convergence rate is in very good agreement with the predicted value (which is a very slow rate due to the high-order of singularity for the problem). It can be seen that the enriched solution yields an error that is about one order of magnitude less than the corresponding FE solution, although retaining the same convergence rate. This behaviour is expected when using uniform refinement with topological enrichment, as has been demonstrated in other LEFM applications with partition of unity enrichment [23, 24].

In Figure 8 (left) it can also be seen that a geometric enrichment greatly improves both the precision of the calculation together with the convergence rate. The geometric enrichment removes the effect of the singularity, recovering the expected convergence rate for a smooth problem. This behaviour is consistent with that obtained in linear elastic fracture mechanics [24].

Figure 8 (right) shows the relative error in the quantity of interest (GSIF) computed for $r_q/d = 0.87$. The improvement obtained with the introduction of the enrichment functions is clear, with a convergence rate greater than the convergence rate of the error in strain energy. As expected, when using geometric enrichment, a more accurate estimation of the GSIF is obtained as well as an improved convergence rate. In this case, the *a priori* error estimate for post-processed functionals (or quantities

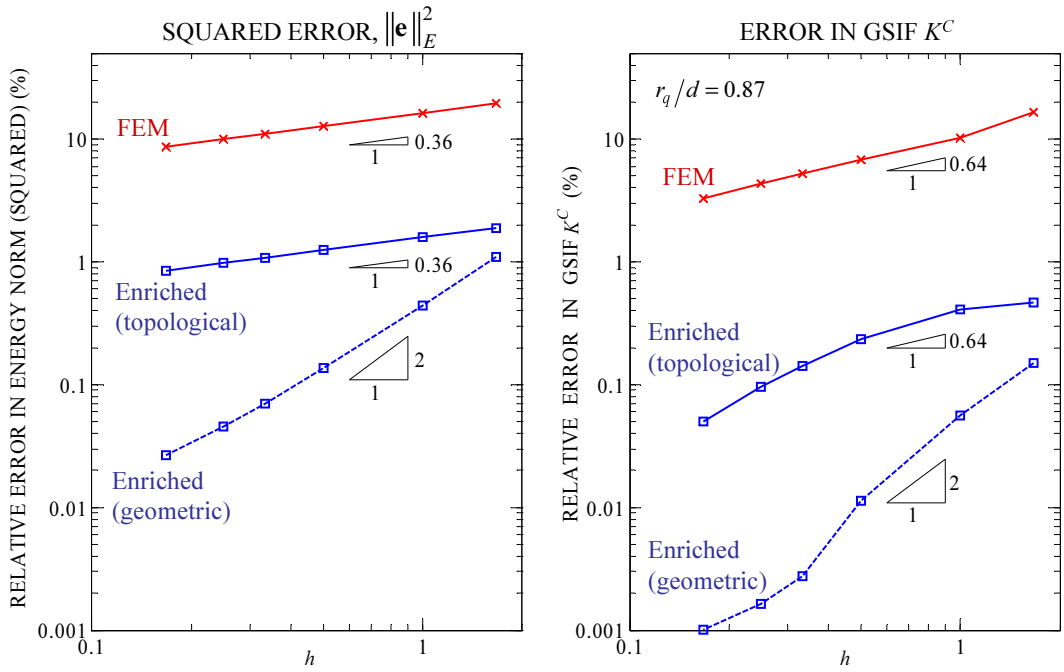

Figure 8. Convergence rates and relative error in energy norm (squared) and in K^C for the sequence of meshes analyzed in Figure 7. In the GSIF computation, the radius of the q-function for all meshes is $r_q/d = 0.87$. A 40×40 Gauss quadrature has been used for the enriched elements.

of interest) is of the form [25, 26]:

$$|K^C - K^{C,h}| \leq \|\mathbf{u} - \mathbf{u}^h\|_E \|\mathbf{z} - \mathbf{z}^h\|_E = \|\mathbf{e}\|_E \|\mathbf{z} - \mathbf{z}^h\|_E, \tag{22}$$

where $\mathbf{z}$ is the exact solution to an auxiliary (or adjoint) problem, $\mathbf{z}^h$ its finite element approximation and $|K^C - K^{C,h}|$ is the error in the computed functional (GSIF). In general, $\|\mathbf{z} - \mathbf{z}^h\|_E$ is of comparable magnitude to $\|\mathbf{e}\|_E$, and hence, the error in the computed functional is of comparable magnitude to the squared error in energy norm, but it also can be much smaller (depending on the functions involved in the auxiliary problem). The results obtained for the error in the GSIF and the convergence rates shown in Figure 8 (right) are in good agreement with this *a priori* estimate.

5.1.4. Effect of quadrature. The number of integration points necessary to properly implement the enriched formulation has been analyzed and the results are shown in Figure 9. The results presented in Figure 8 were computed using a 40×40 Gauss quadrature to guarantee that integration errors do not affect the convergence rate of the error in energy norm for the small errors associated with the geometric enrichment. However, from a practical point of view, a 15×15 quadrature is sufficient when a topological enrichment is used, since it virtually yields the same results as for the 40×40 quadrature. However it cannot guarantee the expected convergence rate for a geometric enrichment. Note that the integration error when using a 5×5 quadrature causes a larger error in energy norm, although the results are always better than the standard FE solution. Obviously, the necessity of a high order of quadrature is due to the highly singular behaviour reproduced by the enrichment functions.

For the aforementioned results the elements of the indenter and specimen do not need any subdivision for integration purposes, since the singular point is always located at the corner node. However, when the indenter slides, the singular point on the specimen can be located along the side between surface nodes (i.e. the mesh is non-conforming). In this case, the enriched element containing the singular point is subdivided into triangles. Figure 9 depicts only the situation in which the singular point is located at a node both in the indenter and in the specimen. Therefore, no subdivision is needed and a Gauss quadrature is employed. However, subdivision into triangles can always be performed and the corresponding results are shown on the same plot for a 73-point integration rule (used for the triangular subdomains next to the singular point in combination with a 15×15 quadrature for the rest of enriched elements). In this case, the squared error in $\|\mathbf{e}\|_E$ for a topological enrichment is again very close to the error when using no subdivision. Similar comments can be made on the effect of the quadrature on the quantity of interest K^C.

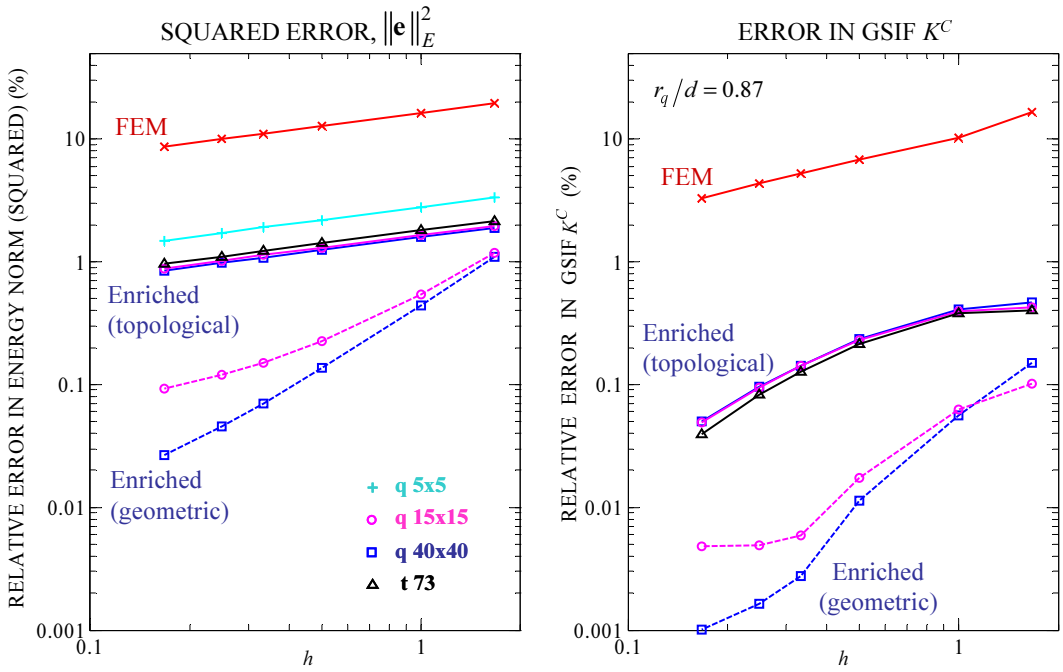

Figure 9. Effect of the number of integration points for the case of the singular point at a node on the specimen side (solid 2). The case of subdivision into triangles with 73 integration points is also considered.

5.2. Problem 2: Application to a sliding contact problem

Figure 10 shows the model used to assess the behaviour of the enrichment under sliding contact conditions. A distributed normal load p is applied on the indenter top. The vertical load is applied to a reference node which is linked to the rest of nodes on the indenter top by means of multipoint constraints (MPCs) to ensure an even load distribution. A displacement ΔU_x is then imposed to the reference node to cause a sliding condition of the whole indenter. Note that this second load step is displacement controlled, so as to guarantee the convergence of the sliding condition. The friction coefficient is $f = -1.6$ (sliding to the left) and the bodies are assumed elastically similar. To model the sliding frictional contact, we have used a Lagrange multiplier formulation. In addition, a Coulomb

friction model has been assumed between the contact surfaces. We recall here that the contact between enriched elements on both sides of the contact surfaces is not directly defined. It is accomplished by means of overlay elements with negligible stiffness that are linked to the enriched nodes, as explained in Section 4.1. Since an exact solution is not available in the literature for this problem, the model

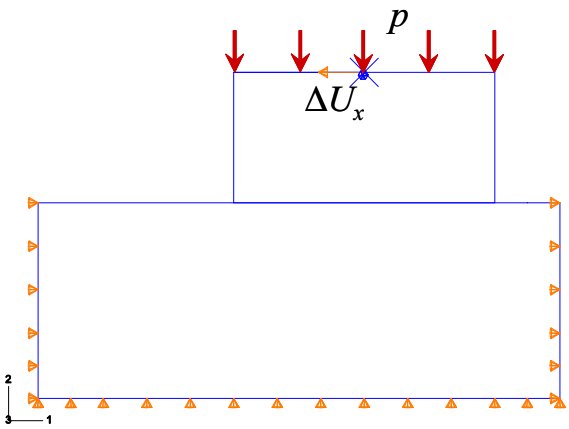

Figure 10. Model of a sliding problem for evaluating the enrichment performance.

was solved using standard FEM with a refined mesh using quadratic elements. This overkill mesh is used as a reference solution and is shown in Figure 11. The GSIFs obtained for different r_q/d with the quadratic mesh were averaged to get a reference value of K^C_{ref}. On the other hand, a coarse mesh was enriched as shown in Figure 11. This coarse mesh was also analyzed with a standard FE approach using only linear elements.

Figure 12 shows the clear improvement achieved when using the enriched formulation, especially when it is compared to the standard FE solution. For the same coarse mesh (348 nodes) the enriched solution (715 dof) is clearly more accurate than the standard bilinear FE solution (651 dof). Moreover, the enriched solution using just 715 dof compares rather favorably with the overkill finite element solutions that contain two orders more of degrees of freedom.

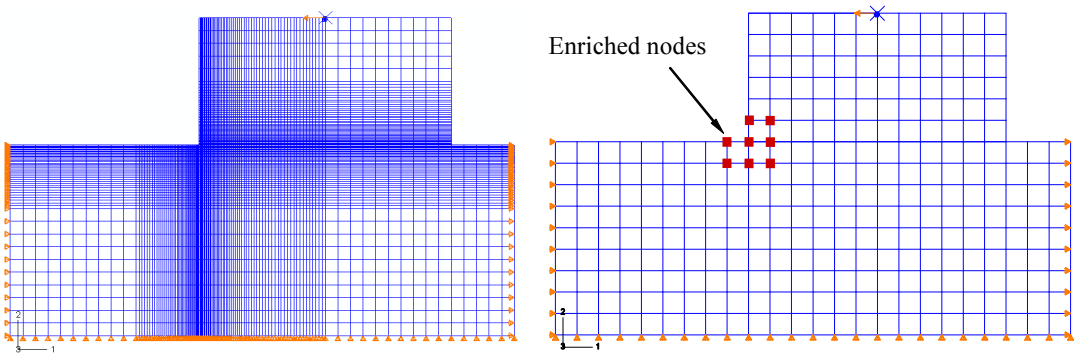

Figure 11. Left, overkill mesh used as a reference solution and analyzed with standard FEM (quadratic elements). Right, coarse mesh analyzed with both standard linear finite elements and with the proposed enrichment.

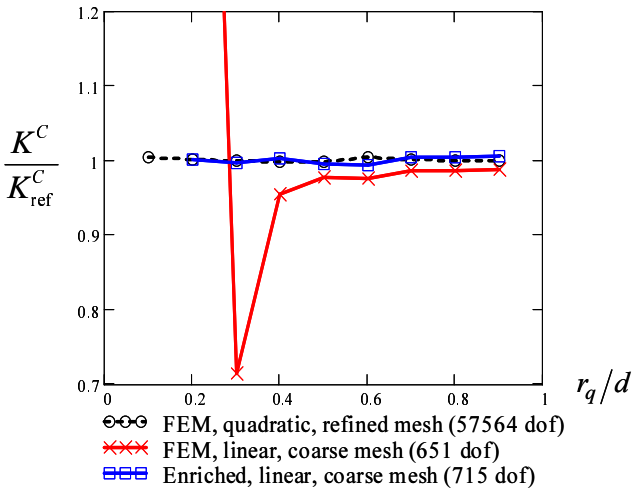

Figure 12. GSIF estimations for the two meshes shown in Figure 11.

6. CONCLUSIONS

In this paper, a new approach to model the singularity in complete contact problems under sliding conditions was presented. We enriched the standard finite element displacement approximations with additional functions through the framework of partition of unity. This was carried out by including

special (enrichment) functions that were based on the *a priori* knowledge of the analytical solution of the singular contact field. These enrichment functions were derived, and a few salient features of their implementation in the commercial code ABAQUS^{TM} were described.

Two numerical examples were presented to assess the performance of the enrichment and the accuracy of the method. A specific domain integral formulation was used to compute the generalized stress intensity factors. Good estimations of the generalized stress intensity factor (GSIF) and the strain energy were obtained, which were consistently much better than the ones obtained with the standard FEM. The convergence rates in energy and in the GSIF were studied for topological and geometric enrichment. Other issues such as the adequate number of integration points were also investigated. The proposed approach enables the use of coarse meshes which is especially important in non-linear contact problems, since it reduces the computational costs. Unlike special singular finite elements where the singular point must be on a node, in the present technique, the singular point can be arbitrarily located along the contact surface of the substrate.

ACKNOWLEDGEMENTS

This work was financially supported by the Ministerio de Educación y Ciencia in the framework of the research project DPI2007-66995-C03-02. The financial support of the Universidad Politécnica de Valencia and the Generalitat Valenciana through the project GV06/124 is also gratefully acknowledged. This support enabled the research visit of E. Giner to UC Davis, where parts of this research were accomplished.

REFERENCES

1. Hills DA, Nowell D. *Mechanics of Fretting Fatigue*. Series: Solid Mechanics and its Application. Kluwer Academic Publishers, Dordrecht, 1994.

2. Williams ML. Stress singularities resulting from various boundary conditions in angular corners of plates in extension. *Journal of Applied Mechanics* 1952; **19**:526–528.
3. Gdoutos EE, Theocaris PS. Stress concentration at the apex of a plane indenter acting on an elastic half-plane. *Journal of Applied Mechanics* 1975; **42**:688–692.
4. Comninou M. Stress singularity at a sharp edge in contact problems with friction. *Journal of Applied Mathematics and Physics (ZAMP)* 1976; **27**:493–499.
5. Mugadu A, Hills DA, Limmer L. An asymptotic approach to crack initiation in fretting fatigue of complete contacts. *Journal of Mechanics and Physics of Solids* 2002; **50**(3):531–547.
6. Giner E, Tur M, Vercher, A, Fuenmayor FJ. Integral de dominio para el cálculo de factores de intensidad de tensiones generalizados en problemas de contacto mediante elementos finitos. In *Métodos Numéricos en Ingeniería 2005*, Eds. J.L. Pérez Aparicio *et al.*, SEMNI-AMPTAC, Granada, Spain, 2005.
7. Tur M, Giner E, Fuenmayor FJ. A contour integral method to compute the generalized stress intensity factor in complete contacts under sliding conditions. *Tribology International* 2006; **39**(10):1074–1083.
8. Fuenmayor FJ, Giner E, Tur M. Extraction of the generalized stress intensity factor in gross sliding complete contacts using a path-independent integral. *Fatigue and Fracture of Engineering Materials and Structures* 2005; **28**(12):1071–1085.
9. Melenk JM, Babuška I. The partition of unity finite element method: Basic theory and applications. *Computer Methods in Applied Mechanics and Engineering* 1996; **139**(1-4): 289–314.
10. Babuška I, Melenk JM. The partition of unity method. *International Journal of Numerical Methods in Engineering* 1997; **40**(4):727–758.
11. Belytschko T, Black T. Elastic crack growth in finite elements with minimal remeshing. *International Journal of Numerical Methods in Engineering* 1999;**45**:601–620.
12. Moës N, Dolbow J, Belytschko T. A finite element method for crack growth without remeshing. *International Journal of Numerical Methods in Engineering* 1999; **46**(1):131–150.
13. Sukumar N, Moës N, Moran B, Belytschko, T. Extended finite element method for three-dimensional crack modelling. *International Journal of Numerical Methods in Engineering* 2000; **48**(11):1549–1570.
14. Strouboulis T, Copps K, Babuška I. The generalized finite element method. *Computer Methods in Applied Mechanics and Engineering* 2001; **190**(32–33):4081–4193.
15. Huang R, Prévost J.-H., Huang ZY, Suo Z. Channel-cracking of thin films with the extended finite element method. *Engineering Fracture Mechanics* 2003; **70**(18):2513–2526.
16. Sukumar N, Huang ZY, Prévost J.-H., Suo Z. Partition of unity enrichment for bimaterial interface cracks. *International Journal of Numerical Methods in Engineering* 2004; **59**(8):1075–1102.

17. Tur M, Fuenmayor J, Mugadu A, Hills DA. On the analysis of singular stress fields - Part 2: Application to complete slipping contacts. *Journal of Strain Analysis and Engineering Design* 2003; **38**(3):207–217.
18. Lee D, Barber JR. An automated procedure for determining asymptotic elastic stress fields at singular points. *Journal of Strain Analysis and Engineering Design* 2006; **41**(4):287–295.
19. Barber JR. *Elasticity*. Kluwer Academic Publishers, Dordrecht, 2002.
20. Tracey DM, Cook TS. Analysis of power type singularities using finite elements. *International Journal of Numerical Methods in Engineering* 1977; **11**:1225–1233.
21. Sukumar N, Prévost J.-H. Modeling quasi-static crack growth with the extended finite element method. Part I: Computer implementation. *International Journal of Solids and Structures* 2003; **40**(26):7513–7537.
22. Belytschko T, Moës N, Usui S, Parimi C. Arbitrary discontinuities in finite elements. *International Journal of Numerical Methods in Engineering* 2001; **50**:993–1013.
23. Béchet E, Minnebo H, Moës N, Burgardt B. Improved implementation and robustness study of the X-FEM for stress analysis around cracks. *International Journal of Numerical Methods in Engineering* 2005; **64**(8):1033–1056.
24. Laborde P, Pommier J, Renard Y, Salaün M. High-order extended finite element method for cracked domains. *International Journal of Numerical Methods in Engineering* 2005; **64**:354–381.
25. Babuška I, Miller A. The post-processing approach in the finite element method. Part 2: The calculation of stress intensity factors. *International Journal of Numerical Methods in Engineering* 1984; **20**:1111–1129.
26. Szabó B, Babuška I. *Finite Element Analysis*. John Wiley & Sons, New York, 1991.